Nonlinear interaction between clustered unstable thermoacoustic modes in can-annular combustors

Jakob G. R. von Saldern[a], Jonas P. Moeck[b], Alessandro Orchini[a,*]

[a] *TU Berlin, Institute of Fluid Dynamics and Technical Acoustics, Müller Breslau Str. 8, 10623 Berlin, Germany*
[b] *Norwegian University of Science and Technology, Department of Energy and Process Engineering, 7491 Trondheim, Norway*

Abstract

A can-annular combustor consists of a set of nominally identical cans, in which the flames burn in an essentially isolated manner. However, adjacent cans are able to communicate acoustically, which provides dynamic coupling of the entire can-annular arrangement. Recently, it was shown that the acoustic coupling is not negligible and can cause clustering of eigenfrequencies. In this study, we present a low-order modeling framework for self-excited thermoacoustic oscillations in generic can-annular combustors consisting of N identical cans. The dynamics of the flames are modeled with the nonlinear G-equation; the acoustic model accounts for plane acoustic waves inside the cans and can-to-can communication. The latter is enabled through a coupling boundary condition that is based on conservation of mass and a Rayleigh conductivity. For weak coupling between adjacent cans, the thermoacoustic feedback cycle shows clusters of linearly unstable modes of different azimuthal order, which are close in frequency and growth rate. Their interaction in the nonlinear regime is investigated using time-domain simulations. Two simulations for generic can-annular combustors consisting of 4 and 6 cans with weak acoustic coupling are discussed in this study. We observe a strong interaction between the modes, which can cause long transition times and allows modes that do not dominate the system dynamics in the linear regime to be dominant in the nonlinear regime. While the $N = 6$ case converges to a periodic oscillation pattern with one dominant frequency, the $N = 4$ case converges to a quasi-periodic oscillation involving modes of different azimuthal order. Moreover, we observe a synchronization of these modes. These results raise the questions whether it is possible to predict which mode(s) will dominate the system in the saturated state and under which conditions synchronization of clustered modes can occur.

Keywords:
Can-annular combustor, Thermoacoustics, Nonlinear interaction, Weak coupling, Kinematic flame model

*Corresponding author:
Email address: a.orchini@tu-berlin.de (Alessandro Orchini)

1. Introduction

Thermoacoustic oscillations in axial and annular combustors have been studied extensively in the past years [1]. In contrast, can-annular systems have received less attention and have often been regarded as single cans, neglecting any acoustic cross-talk communication. However, recent experimental, theoretical and numerical studies have shown that the acoustic interaction between adjacent cans cannot be neglected, even when it is weak. The acoustic coupling arises from 1) a small gap between adjacent cans in the transition zone to the turbine inlet, and 2) a joint plenum upstream of the combustor. The relevance of can-to-can interaction was first demonstrated in a numerical and experimental study, in which thermoacoustic oscillations in a quarter of a can-annular combustor with 16 cans were examined [2]. The effect of the cross-talk area at the turbine vane section has been investigated numerically in [3]. Only recently, a more comprehensive theoretical study on the thermoacoustics of can-annular combustors has been conducted [4]. It was shown that azimuthal modes also arise in can-annular systems, even for weak acoustic cross-talk communication.The weak acoustic coupling also leads to the formation of eigenvalue clusters with closely spaced frequencies and growth rates. This is a unique feature of can-annular configurations and raises the question, how clusters of linearly unstable thermoacoustic modes will interact in the nonlinear regime, and which mode(s) will eventually dominate.

The formation of eigenvalue clusters is atypical in non-can-annular configurations. Axial single-flame combustors generically have non-closely spaced eigenfrequencies; theoretical and experimental studies have shown that when more than one mode is unstable, either one suppresses the other(s), resulting in a periodic oscillation, or multiple frequencies persist, and a quasi-periodic oscillation manifests [5, 6]. Annular combustors may have closely spaced acoustic eigenfrequencies, depending on the specific geometrical dimensions of the combustor. For example, it can then happen that two thermoacoustic modes, one of azimuthal and one of longitudinal nature, exist at close frequencies and are simultaneously unstable. The interaction between an axisymmetric and an azimuthal mode, manifesting in an oscillation pattern known as slanted mode [7], was theoretically examined in [8], and it was suggested that two closely spaced eigenfrequencies can synchronize. More formal conditions on whether synchronization is possible for closely spaced axial and azimuthal modes were derived in [7]. For a can-annular combustor with N cans and weak acoustic coupling, instead, clustering is a common feature, and a whole cluster of N thermoacoustic modes can be unstable.

When examining can-to-can communication, the simplest configuration that can be considered is an $N = 2$ can setup. Oscillation patterns in which adjacent cans oscillate in-phase (in anti-phase) are called push–push (push–pull) modes. In [9], push–push, push–pull and bi-modal oscillations were observed in an experimental setup formed by two cans acoustically coupled downstream via a cross-talk tube aligned normal to the flow direction. Real gas turbines, however, usually feature a larger number of cans. This leads to a larger number of modes in a cluster and allows for the formation of more possible acoustic oscillation patterns.

The study aims to numerically investigate fundamental features of can-annular combustors with a weak acoustic coupling between adjacent cans. For this purpose, we develop a generic acoustic wave-based can-annular combustor model consisting of N identical cans, which are acoustically connected at the downstream end. The acoustic response is then represented as a low-order state-space model. This is coupled with a nonlinear dynamical flame model based on the G-equation in each can [10]. In the weak coupling scenario, clusters of linearly unstable modes can be observed, which are closely spaced in frequency and growth rate but have very different mode shapes. We find that, due to the close spacing between the eigenvalues, the nonlinear interaction between the modes is strong. This manifests in pronounced beating patterns during the transient and can lead to synchronization between some of the unstable modes.

2. Thermoacoustic model

The nonlinear flame and heat release rate dynamics are modeled numerically in this study using LSGEN, a C-based level set solver for the kinematic G-equation. So far, the code has been used to investigate thermoacoustic phenomena with only one flame, by coupling the flame dynamics with a single-input single-output acoustic state space model of an axial-type combustor [6]. For the present study, LSGEN has been extended to model annular and can-annular combustors with an arbitrary number of flames. This is achieved by solving multiple G-equations simultaneously (one flame for each can), whose dynamics are coupled by a multi-input multi-output acoustic state-space model that represents an annular or a can-annular configuration. General details on LSGEN and its implementation can be found in [5, 6]. Here, we describe only the key equations and their extension to multi-flame combustion systems. In the following, we present the nonlinear thermoacoustic model

consisting of the nonlinear G-equation, which tracks the evolution of the flame front in implicit form, and the linear acoustic model. How these equations can be used to also examine linear stability is briefly discussed in §3. Note that we consider a generic configuration and do not attempt reproducing experimental data.

2.1. Flame dynamics

We model a generic annular/can-annular combustor with N identical flames equally distributed along the azimuthal direction. Assuming fully premixed, axisymmetric, conical flames with base radius of 5.5 mm, the G-equation for each flame j reads

$$\frac{\partial G_j}{\partial t} + \left[\mathbf{u}_j - s_l \frac{\nabla G_j}{|\nabla G_j|}\right] \cdot \nabla G_j = 0. \tag{1}$$

The flame front is convected by the underlying flow velocity $\mathbf{u}_j = [\bar{u}_x + u'_{x,j}, u'_{r,j}, 0]$, which is assumed to have only a mean component in the axial direction, $\bar{u}_x = 1.5$ m/s. The flame front propagates normally to the flame surface with speed $s_l = 0.47$ m/s. In order to resolve the flame dynamics, the underlying perturbed velocity field must be appropriately modeled [11]. For each flame, axial acoustic fluctuations impinging the burner outlet cause the formation of coherent structures at the burner edges, which propagate into the flame field:

$$\frac{\partial u'_{x,j}}{\partial t} + U_{\text{ad}} \frac{\partial u'_{x,j}}{\partial x} = 0, \qquad u'_{x,j}(x = 0, t) = u'_{\text{ac},j}, \tag{2}$$

where U_{ad} is the fluctuation advection speed, which is set to $0.83\bar{u}_x$ [12]. Velocity fluctuations in the radial direction are imposed by conservation of mass:

$$\frac{1}{r}\frac{\partial (r u'_{r,j})}{\partial r} + \frac{\partial u'_{x,j}}{\partial x} = 0, \qquad u'_{r,j}(r = 0, t) = 0. \tag{3}$$

The unsteady heat release can be computed as

$$q_j(t) = 2\pi\rho h_R \iint_{\mathcal{D}} s_l |\nabla G_j| \delta(G_j) r \, \mathrm{d}r \, \mathrm{d}x, \tag{4}$$

where δ is the Dirac delta function, ρ the unburned gas density and h_R the reaction enthalpy [13]. The mean heat release is determined by the temperature jump across the flame.

This set of equations is solved simultaneously for every flame ($j = 1 \ldots N$) in the generic thermoacoustic acoustic model. The flame model resolves nonlinear effects, including the formation of cusps and pinch-offs, as shown in [6]. Although no direct flame-to-flame interaction is considered (which is the case in a can-annular combustor), the flames' dynamics are indirectly coupled by the interaction between the heat release rates and the acoustic response of the entire configuration.

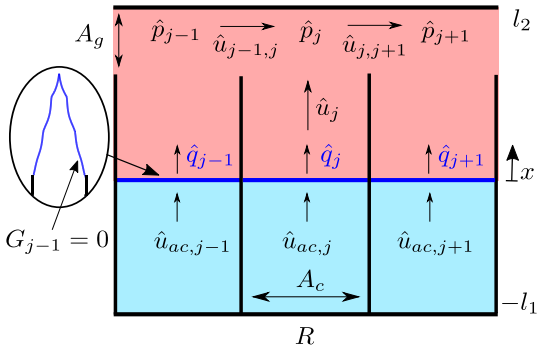

Figure 1: Sketch of three adjacent cans. Periodic boundary conditions set can $j = N + 1$ to be can $j = 1$.

2.2. Multi-input multi-output acoustic response

To model the acoustics in a can-annular combustor, we assume that only plane waves propagate in each can. All cans are assumed to be identical. The unsteady heat release in each can is considered as a compact acoustic source term, as shown in Fig. 1. Mean flow properties are assumed to be constant upstream/downstream of the flame. The mean temperature is set to $T_{\text{up}} = 300$ K upstream of the flame, and it changes by a factor of two across the flame. The mean upstream velocity and pressure are set to 1.5 m/s and 1 bar, respectively. Other mean quantities can be determined by conservation of mass, momentum and energy, and by the state equation of an ideal gas with gas constant $R_{\text{gas}} = 287$ J/(kg K) and ratio of specific heats $\gamma = 1.4$. The speed of sound is given by $c = \sqrt{\gamma R_{\text{gas}} T}$.

As customary, we consider a modal decomposition of the acoustic waves in the frequency domain as

$$u'_j(x, t) = \hat{u}_j(x) e^{st} = \frac{1}{\rho c}\left(f_j e^{-\frac{xs}{c+\bar{u}}} - g_j e^{+\frac{xs}{c-\bar{u}}}\right) e^{st}, \tag{5}$$

where $s = \sigma + i\omega$ is the complex frequency, and f_j (g_j) are the amplitudes of the downstream (upstream) traveling waves in can j. The Rankine–Hugoniot jump conditions are imposed across the flame element [[14]], and the model is closed by applying boundary conditions at the can ends: on the upstream boundary we set the reflection coefficient to $R = 0.95$ – to introduce some damping; on the downstream end, a boundary condition that couples adjacent cans is applied.

We account for the can-to-can communication by allowing for acoustic flux communication between adjacent cans. We derive a coupling boundary condition based on mass conservation and the Rayleigh conductivity. We consider small connection gaps with area A_g at the downstream end as sketched in Fig. 1. By assuming that the connection gaps are acoustically compact,

density fluctuations can be neglected, and acoustic flux conservation then yields

$$\hat{u}_j A_c + \hat{u}_{j-1,j} A_g - \hat{u}_{j,j+1} A_g = 0, \text{ at } x = l_2 = 0.8\text{m}, \quad (6)$$

where A_c is the cross-sectional can area corresponding to a radius of $r_c = 50$ mm. The total length of the cans is 1 m. Note that the cans are assumed to be acoustically closed downstream in the absence of can-to-can interaction, i.e. when $A_g = 0$. To relate the acoustic pressure fluctuations between adjacent cans, we employ the Rayleigh conductivity [15, 16]

$$K_R = -\frac{s\hat{u}_{j,j+1}\rho A_g}{\hat{p}_{j+1} - \hat{p}_j}, \quad \text{at } x = l_2. \quad (7)$$

The strength of the coupling is determined by the gap size and the conductivity K_R. The latter generally depends on the oscillation frequency, mean flow properties and gap geometry [17, 18]. In this study, we neglect mean flow effects and the thickness of the walls between the cans. We assume that the gaps have a circular form, with radius r_g. Under these assumptions, the Rayleigh conductivity is well approximated by $K_R = 2r_g$ [17, 18]. Substituting Eq. (7) into Eq. (6) yields

$$\hat{u}_j A_c - \frac{2r_g}{s\rho}(2\hat{p}_j - \hat{p}_{j-1} - \hat{p}_{j+1}) = 0 \quad \text{at } x = l_2, \quad (8)$$

which is a coupling boundary condition that enables acoustic cross-talk between adjacent cans. Equation (8) allows us to model the acoustics of a generic can-annular combustor with a low-order acoustic model that, despite considering only axial waves in the cans, also describes azimuthal modes, found when the cans do not oscillate in phase.

By combining the upstream/downstream boundary conditions, unsteady flame jump conditions, and wave propagation equations in each can, we obtain a sparse linear system of equations that describes the coupled can-annular thermoacoustic system. It depends on the complex-valued frequency s and has N heat release source terms, one per can. It can be written as

$$\mathcal{A}(s)\mathbf{p} = \mathbf{q}, \quad (9)$$

where the vector $\mathbf{p}$ contains the up- and downstream traveling acoustic wave amplitudes f_j and g_j of all the cans, and $\mathbf{q}$ contains the amplitudes of the heat release rates $\hat{q}_j$. The matrix $\mathcal{A}(s)$ in Eq. (9) is a transfer matrix whose entries relate the acoustic response of the can-annular system to a forced perturbation of the heat released by the N flames. Furthermore, due to the discrete rotational symmetry, the acoustic response can be extracted from Eq. (9) by forcing the heat released by one flame only, and then exploiting the block-circulant nature of matrix $\mathcal{A}(s)$ [8, 19]. First, by varying the forcing frequency of the heat released in can 1 while setting the heat release in all other cans to zero, we calculate the velocity acoustic response at a reference location in all cans by solving Eq. (9) at $s = i\omega$. We then identify a state-space model corresponding to the calculated acoustic response. This is the single-input multi-output model

$$\dot{\mathbf{x}}_1 = \mathbf{A}\mathbf{x}_1 + \mathbf{B}q_1', \qquad \mathbf{u}_1' = \mathbf{C}\mathbf{x}_1, \quad (10)$$

whose output vector $\mathbf{u}_1' \equiv [u_{1,1}', ..., u_{N,1}']$ contains the contribution to all velocity fluctuations upstream of the flames caused by unsteadiness of the heat source in the first can only, q_1. The matrices $\mathbf{A}, \mathbf{B}, \mathbf{C}$ are identified using the fitting algorithm of [20]. Since all cans are identical, the acoustic response between a forcing heat source and an upstream velocity fluctuation depends only on their distance in number of cans. Thus, the matrices of the identified single-input multi-output state-space model (10) already contain all the information needed to fully characterize the acoustic system. It follows from modular arithmetic and the superposition principle that the total acoustic fluctuation upstream of the flame in the jth can is

$$u_{\text{ac},j}' = \sum_{k=1}^{j} \mathbf{c}_{j-k+1}\mathbf{x}_k + \sum_{k=j+1}^{N} \mathbf{c}_{N+j-k+1}\mathbf{x}_k, \quad (11)$$

where $\mathbf{c}_j$ defines the jth row vector in $\mathbf{C}$ and $\mathbf{x}_k$ is the acoustic state generated by heat release perturbations in can k, calculated from $\dot{\mathbf{x}}_k = \mathbf{A}\mathbf{x}_k + \mathbf{B}q_k'$. This equation feeds as a boundary condition into the flame dynamics, Eq. (2), closing the thermoacoustic model.

Note that the acoustic model is based on plane acoustic waves inside each can and that both the heat source and the coupling gaps are assumed to be acoustically compact. Therefore, the model is only valid for low frequencies.

3. Linear stability and data analysis

Using the can-annular thermoacoustic model presented in §2, we now investigate the effect of the number of cans and of the can-to-can coupling strength on the linear stability and nonlinear dynamics of the can-annular system in the weak coupling range: $\alpha \equiv r_g/r_c \ll 1$. The parameter variation is given by $N = [2, 3, 4, 5, 6]$ and $\alpha = [0.005, 0.01, 0.015, 0.02]$.

Before performing nonlinear time-domain simulations, we examine the linear stability of the thermoacoustic system in frequency domain. This is achieved

by introducing a frequency-domain representation of the linear heat release response in Eq. (9), identical for all flames. The latter is expressed in terms of the Flame Transfer Function (FTF), which was determined numerically by forcing the G-equation with velocity fluctuations at various frequencies with an amplitude of 1% of the mean flow velocity. An FTF extracted from LSGEN can be found in Figure 6 in [6]. Equation (9) then becomes an eigenvalue problem, whose solution yields the thermoacoustic eigenvalues and modes.

Figure 2 shows clusters of unstable eigenfrequencies identified in this way for two different can numbers and various gap radii. The modes can be classified according to their azimuthal mode number, m. As the acoustics within each can are one dimensional, the number of independent azimuthal modes is equal to the number of cans. For a given gap radius, a set of all possible azimuthal modes can be observed within the clusters. It can be seen that the push–push mode frequency ($m = 0$) is insensitive to variations in N and α. This is because this axial mode can be observed in a single-can combustor, and persists for configurations with arbitrary numbers of cans when the acoustics in each can oscillates in phase. Also, the push–pull mode frequencies ($m = N/2$, even N only), which can already be observed in a two-can combustor, do not change when varying the number of cans, although they are affected by the strength of the coupling. The modeshapes of a generic can-annular system analogous to that discussed here can be found in [4]. The distance between the eigenfrequencies is larger when increasing α, leading to less closely spaced clusters. The gray lines in Fig. 2 show the paths along which the modes move for a continuous change in α. This is consistent with considering

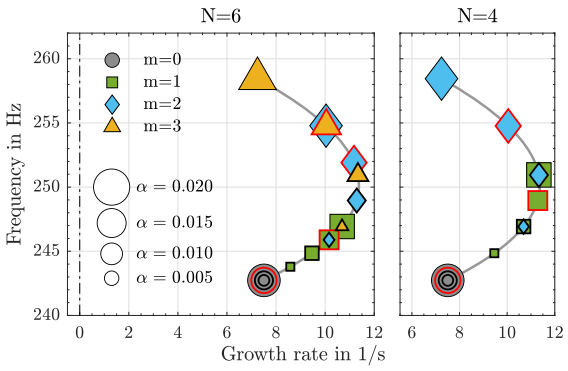

Figure 2: Cluster of unstable eigenfrequencies for $N = 6$ (left) and $N = 4$ (right) and different gap radii. The symbols indicate the azimuthal order and the symbol size indicates the gap radius. The cases for which time domain simulations are discussed are highlighted in red.

a weakly coupled can-annular system in analogy to a set of weakly coupled oscillators. Note that all eigenfrequencies move along the same trajectory starting from the push–push mode, in the limit $\alpha \to 0$. This is because the coupling boundary condition can be interpreted as an effective continuous boundary condition. Since all modes for $m > 0$ stem from the push–push mode, then, if the push–push mode is linearly unstable, all modes for higher azimuthal orders will, for small connection radii, also be unstable. In §4 we discuss in detail the nonlinear dynamics resulting from configurations with $N = 6, \alpha = 0.015$ (case 1) and $N = 4, \alpha = 0.015$ (case 2). The unstable frequencies of these cases, as predicted by the FTF method, are highlighted in red in Fig. 2.

All time-domain computations were initialized with a zero acoustic state and non-perturbed conical flames. The velocity fluctuations upstream of all flames, $u'_{\mathrm{ac},j}$, are stored at every time step, $\Delta t = 0.0165$ ms. Due to the close spacing of the unstable complex frequencies within a cluster, it is difficult to analyze the temporal evolution of the unstable modes with common time series analysis methods such as spectrograms or Hilbert transforms. However, in Fourier space the acoustic velocity field can be written as

$$\hat{u}(x,\theta_j) = \sum_m \hat{u}_m(x,\theta_j) = \sum_m \psi_m(x) e^{im\theta_j}, \qquad (12)$$

where $\theta_j = (j-1)2\pi/N$ is the discrete coordinate in the azimuthal direction and $\psi_m(x)$ is the modal amplitude for a given azimuthal mode number m. Since the acoustics in each can are one dimensional, the azimuthal mode number takes values $m = [0, \pm 1, ..., \pm N/2 - 1, +N/2]$ or $m = [0, \pm 1, ..., \pm(N-1)/2]$ for an even or an odd number of cans, respectively. Note that, in the linear regime, no distinction between $\pm m$ eigenfrequencies can be made, as these pairs correspond to two counter rotating waves with the same eigenvalue [4].

The discrete Fourier formalism enables us to differentiate the dynamics of the closely spaced modes by means of a decomposition in the azimuthal direction of the N velocity time-series. The time-domain dynamics of each mode can then be reconstructed via an inverse Fourier transform that considers only the azimuthal order(s) of interest. This yields a velocity time series in each can for azimuthal orders m from 0 to $N/2$ or $(N-1)/2$ for even or odd N, respectively. Since the processed time series are real valued, so far no distinction between positive (spinning clockwise) and negative (spinning counterclockwise) azimuthal order can be made. This is achieved by first taking the Hilbert transform of each modal time signal, and then using Eq. (12) to solve for the modal amplitudes ψ_m. To avoid spectral

leakage, the time series are band-pass filtered around the frequency of interest (the fundamental frequency of the azimuthal order or its first harmonic in our case, as they contain the dominant peaks in the spectra) before applying the Hilbert transform. The resulting time-resolved azimuthal amplitudes ψ_m show how the linearly unstable modes evolve in the nonlinear feedback cycle.

4. Nonlinear dynamics of can-annular combustors

Depending on the number of cans and the coupling radius considered, the system exhibits different oscillation patterns. In this section we discuss the nonlinear interaction between clustered unstable modes and the time evolution of the modal amplitudes based on the acoustic velocity time series for the two cases discussed in §3. The evolution of the acoustic pressure is analogous to that of the velocity fluctuations and therefore not further discussed.

4.1. Case 1: periodic oscillations of a push–pull mode

Figure 3 shows the first 5 s (out of 20 s simulated) of the non-processed velocity fluctuations $u'_{\mathrm{ac},j}$ in the $N = 6$ cans. In the transient all 6 unstable modes contribute to the dynamics. Due to the closely spaced frequencies of the thermoacoustic modes active in the transient, the velocity time series show a complex interaction between the oscillations in the different cans, and typical beating effects can be observed, which disappear after the transient period. After about 4 s a steady state is reached, in which only one mode persists, and a push–pull oscillation is established. The last 10 s of the time series in can 1 were used to compute the spectrum shown in Fig. 4. It shows that the system reaches a limit cycle with fundamental frequency 256.2 Hz, with a first harmonic contribution.

The evolution of the modal amplitudes, computed with the method outlined in §3, allows for a deeper insight into the transient dynamics and the interaction between the modes. The modal amplitudes are shown in Figs. 5a) and 5b) for the fundamental and first harmonic components, respectively. All linearly unstable modes

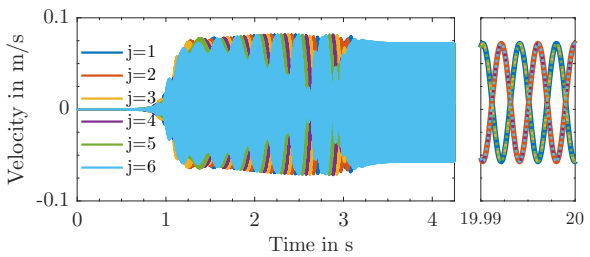

Figure 3: Velocity fluctuations upstream of the flames in all 6 cans. Left: transient. Right: steady state.

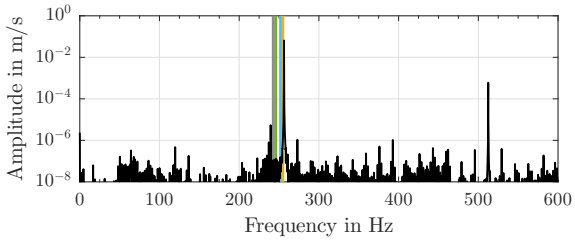

Figure 4: Spectrum of the velocity time series upstream of the flame in the first can. The frequencies of the linearly unstable modes are highlighted with vertical lines. The colors indicate the azimuthal order as in Fig. 2. The frequency resolution is 0.1 Hz.

are independently growing exponentially in the linear regime (until about $t = 1$ s). With increasing amplitude levels, nonlinear effects kick in, and the modes start to interact. As some modes continue growing in amplitude, others are suppressed. Not all modes are suppressed at the same rate. The $m = 2$ mode, which corresponds to the eigenfrequency with the largest growth rate (see Fig. 2), grows the fastest. Its amplitude reaches a maximum at about $t = 1.4$ s and is an order of magnitude larger than that of all other modes; however, rather than saturating to a constant value, it starts decaying afterwards. The $m = 3$ mode, instead, monotonically increases in amplitude at a slower rate and eventually saturates to a fixed amplitude; it is the only mode that persists in the steady-state oscillation. The evolution of the modal amplitudes of the first harmonics (Fig. 5b) is slaved to that of the fundamental frequencies. Note that the azimuthal order of the modes in this frequency region does not correspond to the azimuthal order of the corresponding fundamental mode. The G-equation nonlinearity is dominated by a quadratic term [21]. Thus,

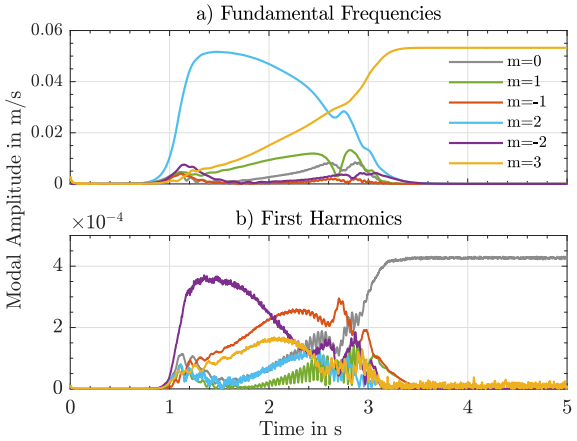

Figure 5: Temporal evolution of the modal amplitudes belonging to an unstable cluster. The time signals are filtered around the a) fundamental frequencies and b) their first harmonics.

the first harmonic of a fundamental oscillation with angular frequency ω and azimuthal order m oscillates at frequency 2ω with azimuthal order $2m$, measured by N sensors as $\mathrm{mod}(2m, N) - NH(\mathrm{mod}(2m, N) - N/2 - 0.5)$ due to aliasing. H is the Heaviside function. The harmonic of the $m = 2$ fundamental mode has therefore azimuthal order $m = -2$, and the harmonic of the $m = 3$ fundamental mode has $m = 0$.

4.2. Case 2: locking between three frequencies

The second case, with $N = 4$, was simulated for about 90 s. The evolution of the modal amplitudes is shown in Fig. 6. In contrast to the previous case, the modal amplitudes reach constant values after a much longer time, at $t = 35$ s. Besides the much longer interaction period, this second case reaches a saturated state in which modes of different azimuthal order are present. Modes of order $m = -1$, 2 and 0 are clearly visible, the mode of order $m = 1$ is suppressed to an amplitude of 2×10^{-4} m/s.

Since multiple modes with close fundamental frequencies survive, the quadratic nonlinearity leads to first harmonic oscillations whose frequencies are linear combinations of all fundamental ones. As a consequence, at a given azimuthal order, more than one frequency is found in the range of the harmonics (for instance frequencies $2f$ and $2f \pm 2\Delta$ all contribute to the $m = 0$ harmonic amplitude). This causes a non-smooth modal amplitude reconstruction with the Hilbert transform. Nevertheless, it can be seen that due to the quadratic term of the nonlinearity, the fundamental $m = -1$ mode strongly feeds a first harmonic oscillation of azimuthal order $m = 2$.

After $t = 35$ s, the simulation was continued further

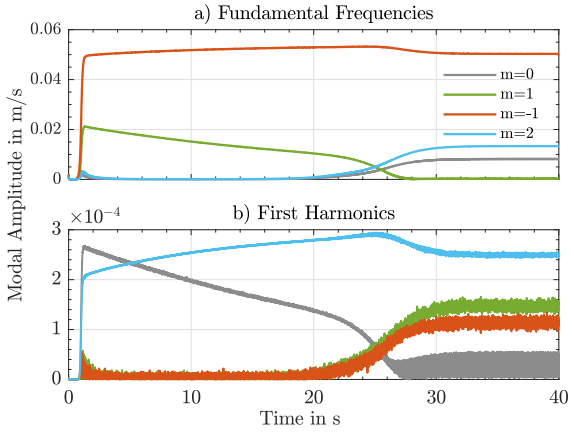

Figure 6: Modal amplitudes, which are computed with the method explained in §3. The upper plot shows the modal amplitudes of the fundamental frequencies and the lower the ones of their first harmonics.

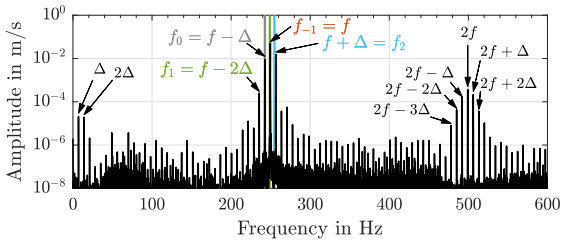

Figure 7: Spectrum of the velocity time series upstream of the flame in the first can. The frequencies of the linearly unstable modes are highlighted with vertical lines. The colors indicate the azimuthal order as in Fig. 6. The frequency resolution is 0.025 Hz.

to provide a highly resolved steady state spectrum. Figure 7 shows the spectrum of the last 40 seconds of the simulation, and Fig. 8 shows the quasi-periodic velocity fluctuations in the four cans for the last 0.05 s. In the linear regime, the $m = 0, 1, 2$ modes were found to have frequencies $f^{\mathrm{lin}}_{0,1,2}$ of 242.7, 249.0 and 254.8 Hz, respectively (see Fig. 2). However, the spectrum corresponding to the nonlinear oscillation state shows three dominant closely spaced frequencies $f_{0,-1,2}$, which in addition are equispaced ($|f_0 - f_{-1}| = |f_{-1} - f_2| = \Delta = 7$ Hz). As a consequence, all frequencies corresponding to peaks in the spectrum can be expressed as linear combinations of only two linearly independent frequencies, such as the frequencies $f = f_{-1}$ and Δ, as shown in Figure 7. This indicates that two of the three modes have synchronized in such a way that their frequencies are now equispaced with respect to the remaining one. Note that the system does not feature any dynamic mode close to $\Delta = 7$ Hz, so that this peak must result from an interaction between the three modes oscillating at finite amplitude.

The peaks in the fundamental frequency range can be directly related to the amplitudes in Fig. 6, but, due to synchronization, the peaks in the first harmonic range cannot be related directly to a unique interaction between the fundamental frequencies. For example, the $2f$ harmonic frequency arises from the interaction of the mode with fundamental frequency f with itself, but also from the interaction between the modes with fre-

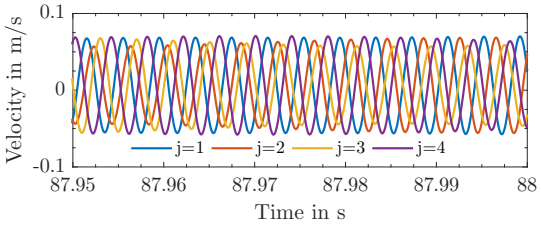

Figure 8: Acoustic velocities upstream of the flames.

quencies $f_0 = f - \Delta$ and $f_2 = f + \Delta$.

5. Discussion and conclusion

In this study we developed a low-order model that simulates self-excited thermoacoustic oscillations in a generic can-annular combustor consisting of N cans. The acoustic model consists of plane acoustic waves inside the cans and can-to-can communication. The latter is established through a coupling boundary condition that is based on conservation of mass and the Rayleigh conductivity. For increasing coupling strength between the cans, thermoacoustic eigenfrequencies of azimuthal order $m \neq 0$ grow out of the $m = 0$ eigenfrequency, which also exists for a single-can system. As a result, the eigenfrequencies appear in clusters for small coupling radii. This implies that if cans are designed in such a way that their thermoacoustic eigenfrequencies have a large negative growth rate, also the eigenfrequencies of a corresponding can-annular system with weak acoustic coupling will have negative growth rates. On the other hand, if a $m = 0$ eigenfrequency of an isolated can is linearly unstable with a large positive growth rate, a respective weakly coupled can-annular system will show a cluster of linearly unstable eigenfrequencies.

The nonlinear interaction of multiple unstable modes in clusters was investigated in the time domain by considering two parameter combinations. Due to the close spacing of the eigenfrequencies, the various linearly unstable modes show a complex interaction in the nonlinear regime. The time until a saturated state is reached is generally relatively long, due to the slow time scale induced by the beating of closely spaced frequencies. It was shown that it is not necessarily the mode with the largest growth rate that dominates the system in the saturated state. While a limit cycle manifests in the first case, the second case shows a multi-mode oscillation involving three different azimuthal orders and giving rise to a non-periodic oscillation pattern. The oscillation frequencies of these modes have synchronized, so that the spectrum only shows two linearly independent frequencies. When only one fundamental frequency contributes to the oscillations, the azimuthal order of the first harmonic frequency is uniquely determined by the leading term of the nonlinearity, which is quadratic for the G-equation. This is however not true for non-periodic oscillations, and the interaction between all oscillating modes needs to be considered. In summary, it was shown that a cluster of linearly unstable modes can cause a complex and relatively slow mode-interaction transient, in which modes of different azimuthal order can also synchronize. So far, the effects of initial conditions have not been considered, although they likely have a role in determining the route undertaken and the steady state reached by the system.

Acknowledgments

JvS is grateful to the ERASMUS+ program and the Studienstiftung des Deutschen Volkes for financial support. AO thanks the DFG (Project Nr. 422037803) for funding his position as PI.

References

[1] A. P. Dowling, S. R. Stow, Acoustic analysis of gas turbine combustors, J Propul Power 19 (2003) 751–764.

[2] P. Kaufmann, W. Krebs, R. Valdes, U. Wever, 3d thermoacoustic properties of single can and multi can combustor configurations, in: ASME Turbo Expo, 2008, pp. 527–538.

[3] F. Farisco, L. Panek, J. B. Kok, Thermo-acoustic cross-talk between cans in a can-annular combustor, Int J Spray Combust 9 (2017) 452–469.

[4] G. Ghirardo, C. Di Giovine, J. P. Moeck, M. R. Bothien, Thermoacoustics of Can-Annular Combustors, J Eng Gas Turb Power 141 (2018) 011007.

[5] I. C. Waugh, K. Kashinath, M. P. Juniper, Matrix-free continuation of limit cycles and their bifurcations for a ducted premixed flame, J Fluid Mech 759 (2014) 1–27.

[6] A. Orchini, S. Illingworth, M. Juniper, Frequency domain and time domain analysis of thermoacoustic oscillations with wave-based acoustics, J Fluid Mech 775 (2015) 387–414.

[7] J. P. Moeck, D. Durox, T. Schuller, S. Candel, Nonlinear thermoacoustic mode synchronization in annular combustors, P Combust Inst 37 (2019) 5343 – 5350.

[8] A. Orchini, G. A. Mensah, J. P. Moeck, Effects of Nonlinear Modal Interactions on the Thermoacoustic Stability of Annular Combustors, J Eng Gas Turb Power 141 (2018) 021002.

[9] K. Moon, H. Jegal, J. Gu, K. T. Kim, Combustion-acoustic interactions through cross-talk area between adjacent model gas turbine combustors, Combust Flame 202 (2019) 405 – 416.

[10] M. Fleifil, A. M. Annaswamy, Z. Ghoneim, A. F. Ghoniem, Response of a laminar premixed flame to flow oscillations: A kinematic model and thermoacoustic instability results, Combust and Flame 106 (4) (1996) 487–510.

[11] T. Schuller, S. Ducruix, D. Durox, S. Candel, Modeling tools for the prediction of premixed flame transfer functions, P Combust Inst 29 (1) (2002) 107–113.

[12] K. Kashinath, S. Hemchandra, M. P. Juniper, Nonlinear thermoacoustics of ducted premixed flames: the influence of perturbation convection speed, Combust Flame 160 (2013) 2856–2865.

[13] T. Lieuwen, Modeling premixed combustion–acoustic wave interactions: A review, J Propul Power 19 (2003) 765–781.

[14] B.-T. Chu, On the generation of pressure waves at a plane flame front, in: Symposium (International) on Combustion, Vol. 4, Elsevier, 1953, pp. 603–612.

[15] J. W. S. Rayleigh, The theory of sound, Vol. 2, Dover, 1945.

[16] M. Howe, On the theory of unsteady high Reynolds number flow through a circular aperture, P Roy Soc Lond A Mat 366 (1979) 205–223.

[17] T. Luong, M. Howe, R. McGowan, On the Rayleigh conductivity of a bias-flow aperture, J Fluid Struct 21 (2005) 769–778.

[18] M. Howe, M. Scott, S. Sipcic, The influence of tangential mean flow on the Rayleigh conductivity of an aperture, P Roy Soc Lond A Mat 452 (1996) 2303–2317.

[19] R. M. Gray, et al., Toeplitz and circulant matrices: A review, Foundations and Trends® in Communications and Information

Theory 2 (2006) 155–239.
[20] B. Gustavsen, A. Semlyen, Rational approximation of frequency domain responses by vector fitting, IEEE Transactions on power delivery 14 (1999) 1052–1061.
[21] Preetham, H. Santosh, T. Lieuwen, Dynamics of laminar premixed flames forced by harmonic velocity disturbances, J Propul Power 24 (2008) 1390–1402.